Conserved L464 in p97 D1-D2 linker is critical for p97 cofactor regulated ATPase activity

Xiaoyi Zhang[1#], Lin Gui[1#], Shan Li[1,2#], Purbasha Nandi[3,4#], Rod Carlo Columbres[1,2], Daniel E. Wong[1], Derek R. Moen[1], Henry J. Lin[1], Po-Lin Chiu[3,4*], and Tsui-Fen Chou*[1,2]

[1] Division of Medical Genetics, Department of Pediatrics, Harbor-UCLA Medical Center and The Lundquist Institute, Torrance, California 90502, USA.

2 Division of Biology and Biological Engineering, California Institute of Technology, Pasadena, California 91125, USA

[3] School of Molecular Sciences, Arizona State University, Tempe, Arizona 85287, USA.

[4] Center for Applied Structural Discovery, The Biodesign Institute, Arizona State University, Tempe, Arizona, 85287, USA.

[#]These authors contributed equally to this work.

*Corresponding author: Po-Lin Chiu (plchiu@asu.edu) and Tsui-Fen Chou (tfchou@caltech.edu) and Division of Biology and Biological Engineering, California Institute of Technology, Pasadena, California 91125, USA. Tel: 1-626-395-6772

Abstract

p97 protein is a highly conserved, abundant, functionally diverse, structurally dynamic homohexameric AAA enzyme-containing N, D1, and D2 domains. A truncated p97 protein containing the N and D1 domains and the D1-D2 linker (ND1L) exhibits 79% of wild-type (WT) ATPase activity whereas the ND1 domain alone without the linker only has 2% of WT activity. To investigate the relationship between the D1-D2 linker and the D1 domain, we produced p97 ND1L mutants and demonstrated that this 22-residue linker region is essential for D1 ATPase activity. The conserved amino acid leucine 464 (L464) is critical for regulating D1 and D2 ATPase activity by p97 cofactors p37, p47, and Npl4-Ufd1 (NU). Changing leucine to alanine, proline, or glutamate increased the maximum rate of ATP turnover (k_{cat}) of p47-regulated ATPase activities for these mutants, but not for WT. p37 and p47 increased the k_{cat} of the proline substituted linker, suggesting that they induced linker conformations facilitating ATP hydrolysis. NU inhibited D1 ATPase activities of WT and mutant ND1L proteins, but activated D2 ATPase activity of full-length p97. To further understand the mutant mechanism, we used single-particle cryo-EM to visualize the full-length $p97^{L464P}$ and revealed the conformational change of the D1-D2 linker, resulting in a movement of the helix-turn-helix motif (543-569). Taken together with the biochemical and structural results we conclude that the linker helps maintain D1 in a competent conformation and relays the communication to/from the N-domain to the D1 and D2 ATPase domains, which are ~50 Å away.

Introduction

p97, also known as VCP (valosin-containing protein), TER (translational endoplasmic reticulum ATPase, in mammals), VAT (valosin-containing protein-like ATPase of *Thermoplasma acidophilum*, in archaea) and Cdc48p (in yeast), is a ubiquitous type II ATPase protein. It is highly conserved and plays essential roles in multiple cellular processes, including protein quality and cell cycle control [1-5], ubiquitin-proteasome system (UPS) [6, 7], transcriptional activation [8], DNA-damage repair [9] and autophagy [10-13]. The involvement of p97 in all major proteolysis pathways makes it a central player in cellular homeostasis. Given its prominent role in eukaryotic cells, p97 malfunction is associated with human disease [14-17]. Single amino acid mutations in p97 (e.g., R155H, Fig. 1A) cause multisystem proteinopathy type 1 (MSP1), also known as inclusion body myopathy with early-onset Paget disease of the bone and frontotemporal dementia (IBMPFD). Some p97 mutations caused amyotrophic lateral sclerosis (ALS) [18]. Variants in p97 have been identified in 2% of familial IBMPFD cases [19-21].

p97 is a 540-kDa homo-hexamer (6×89 kDa) in which each monomer contains an N-terminal domain (NTD, residues 1-184) and two tandem AAA+ ATPase domains, D1 (residues 211-459) and D2 (residues 482-762) domains, and a C-terminal tail (residues 763 to 806) (Fig. 1A). The D1 and D2 domains contain highly conserved Walker A and B motifs and a second region of homology (SRH). During an ATPase cycle, the D2 domain undergoes significant conformational changes, whereas ATP hydrolysis induces only minor changes in D1. The D1 domain is required to form stable hexamers, regardless of the nucleotide-binding state [22, 23]. Cooperativity between the D1 and D2 domains is essential for competent ATPase function [24]. However, the mechanisms of motion transmission and crosstalk between the two domains remain to be elucidated.

Both D1 and D2 domains are organized into a double-ring structure. Cryo-EM structures of full-length p97 showed that the NTD adopts positions up-conformation, down-conformation, and mobile [25, 26]. The NTD binds to various p97 cofactors, which coordinate p97 involvement in major cellular pathways. The largest group of known p97 cofactors are proteins that contain a ubiquitin-regulatory X (UBX) domain (13 members) [27]. The group is further subdivided based on the presence of an N-terminal ubiquitin-associated (UBA) domain, versus UBX-only proteins. Examples are p37 (UBX-only) and p47 (UBA-UBX) [27, 28]. The UBA domain binds the ubiquitinated substrates, and the UBX domain mediates interactions with p97. p47 was the first discovered p97 UBX cofactor and is required for p97-mediated membrane fusion [29, 30]. p37 is highly homologous to p47 in protein sequences but is involved in distinct pathways required for Golgi and endoplasmic reticulum (ER) biogenesis [31]. One of well-characterized p97 cofactors is a heterodimer of Npl4 and Ufd1 (NU). It binds to p97 at distinct sites to form a complex with the stoichiometry of one NU heterodimer per p97 hexamer and is involved in p97-dependent processes [32-35]. Npl4 is an effective target of the potential anti-cancer drug, disulfiram [36, 37].

The N-D1 linker (residues 185-210) and the D1-D2 linker (residues 460-481) connect NTD-D1 and D1-D2 domains, respectively (Fig. 1A). This structural arrangement is also found in another AAA ATPase, N-ethylmaleimide-sensitive factor (NSF), the closest homolog of p97. In NSF, the N-D1 linker is involved in motion transmission from the D1 domain to the N-domain, as well as auto-inhibition of NSF activity [38]. Previous work on p97 suggests that flexibility in the D1-D2 linker region is required for ATP hydrolysis-dependent motion transmission between D1 and D2. Mutations in this region lead to the accumulation of an

endoplasmic reticulum-associated degradation (ERAD) substrate, T cell receptor alpha chain fused to GFP (TCR-α-GFP) [39, 40]. p97 proteins containing only the NTD and D1 domains without the D1-D2 linker domain (ND1) exhibit only 1.4% of the ATPase activity of the full-length wild-type p97 ($p97^{WT}$) protein. In contrast, NTD and D1 domains containing the D1-D2 linker (ND1L) exhibit 79% of $p97^{WT}$ activity [24]. Thus, the linker region is crucial for D1 ATPase competence, but it is unclear how the D1-D2 linker contributes to D1 ATPase activity.

The D1-D2 linker region of p97 is important for motion transmission and D1 activity [39-41]. Tang and Xia reported that the linker activates D1 by breaking the six-fold symmetry of the D1 ring and that half of the D1-D2 linker region is highly conserved from humans to fungi [42]. Our work showed that disease-causing mutations in p97 are associated with improper cofactor-dependent regulation of ATPase activity, demonstrating the importance of cofactor regulation to p97 function [43]. In addition, MSP1 disease mutations caused differential binding of adaptor proteins (p37 and p47) to the NTD of p97 in cells [44, 45].

The present study connects these areas of p97 mechanics by evaluating D1-D2 linker region participation in cofactor-regulated ATPase activity and in regulating the N-domain conformation via solving full-length $p97^{L464P}$ structures using single-particle cryo-EM. We studied the effect of three p97 cofactors on D1-D2 linker mutants constructed from full-length p97 and on a truncated p97 protein containing the N and D1 domains and the D1-D2 linker (ND1L). Our results suggest that the D1-D2 linker region of WT p97 has essential roles in cofactor-regulated ATPase function and its conformation changes will relay to the N-domains, D1 and D2 ATP binding sites. This provides further insight into why p97 mutants cause the accumulation of the ERAD substrate TCR-α-GFP [39], and highlights the importance of linker region in cofactors-regulated p97 ATPase function.

Results

L464 mutations affect the degradation of ubiquitin-proteasome substrate Ub^{G76V}-GFP

The N-D1 linker and the D1-D2 linker (residues 460-481) connect NTD-D1 and D1-D2 domains (Fig. 1A). The p97 crystal structure features an NTD linked to two stacked AAA domains (Fig. 1B). The NTD binding site for p47-UBX (pink; Fig. 1C) resides 37.4 Å and 51.6 Å away from the D1 and D2 nucleotide binding sites, respectively. Therefore, cofactor regulation of ATPase kinetics must involve interactions relayed through the NTD, D1, and D2 domains, as well as the linker regions. We are intrigued by the interesting model and the result suggested that the D1-D2 linker region of p97 is important for motion transmission and to activate D1 activity [39-41]. Li and coworkers demonstrated that p97 mutants L464A, L464E and L464P cause substantial accumulation of TCR-α-GFP, indicating a dramatic loss of ERAD activity [39]. To determine whether the L464 amino acid is critical for the degradation of another p97 dependent proteasome substrate, we expressed L464A, L464E or L464P p97 plasmids in HeLa cells that stably expressed Ub^{G76V}-GFP [46]. We observed an accumulation of Ub^{G76V}-GFP in the L464A, L464E and L464P mutants. We used a p97 ATPase dead mutant as a positive control, which was created by mutating the conserved glutamate residues of the Walker B motifs to glutamines in both the D1 and D2 domains and resulting in single mutants D1-E305Q and D2-E578Q. The mutants were then combined as a double mutant D1-E305Q/D2-E578Q (QQ). This led to the double mutant that allows to bind ATP but is defective in hydrolysis [47]. Strong accumulation of Ub^{G76V}-GFP was also observed in QQ, the ATPase dead mutant. (Fig. S1). We confirmed that the conserved L464 is a critical amino acid for p97 to maintain its role in mediating degradation of p97-dependent ubiquitin-proteasome substrates Ub^{G76V}-GFP [48]. These results suggest that the structural arrangement at position

464 is crucial for proper p97 function, we then evaluated the biochemical and structural effect of L464 by study the effect on cofactor regulated ATPase activity of these mutants. We selected three previously studied cofactors, p47, p37 and Npl4-Ufd1 [43, 49].

D1-D2 linker mutants are defective in p47 regulated p97 ATPase activity

We and others have previously used cofactor regulated ATPase activity as a function readout of cofactor binding to N-domain and communicate to D1 and D2 activity activities [43, 49]. To evaluate whether the conserved L464 is critical for the cofactor-regulated p97 ATPase activity, we purified full-length L464A, L464E and L464P p97 mutants. Consistent with previous reports [39], we found that the basal ATPase activity of mutants L464A and L464E was similar to that of $p97^{WT}$ (Fig. 2A). However, the proline mutant L464P had a two-fold reduction in basal ATPase activity (49% of $p97^{WT}$), suggesting that the proline side chain possibly changes the D1-D2 linker conformation thereby reducing the basal ATP hydrolysis of p97 [40]. We then performed cofactor titration experiments on these three L464 mutants to determine the effects of these mutations on cofactor-regulated ATPase activity. Regulation of $p97^{WT}$ activity by p47 is biphasic, with strong inhibition at lower concentrations of p47 (Phase 1), and less inhibition at higher stoichiometries of the cofactor (Phase 2, or the "rebound" phase) [43]. With the three L464 mutants, however, Phase 1 inhibition at low concentrations of p47 was abolished (Fig. 2B), suggesting that this conserved residue is required for proper cofactor-regulation of the D1 and D2 domains. Moreover, during Phase 2, a >2.2-fold increase in ATPase activity was observed for $p97^{L464A}$ and $p97^{L464E}$ and 3.8-fold increase was for $p97^{L464P}$ -- far beyond the usual $p97^{WT}$ level (0.8-fold). It appears that the conserved L464 residue within the D1-D2 linker plays an important role in p47-regulated p97 ATPase activity. This p47 concentration-dependent effect is similar to that of the D1-E305Q mutant, in which the D1 ATPase is unable to perform ATP hydrolysis (Fig. S2A). Thus, the linker mutants seem to block communication between D1 and D2, and the L464 linker residue is critical for mediating D2 domain cross inhibition by D1 during p47 binding.

L464 mutants display p37 and NU activation profiles similar to those for $p97^{WT}$

Instead of biphasic regulation of p47, we have shown that p37, a p47 homolog, activates the $p97^{WT}$ function (4.2-fold) [31, 43]. In the presence of p37, the D1-D2 linker mutants followed an activation profile similar to profiles for $p97^{WT}$. L464A and L464E had slightly decreased activation by p37 (3.1- and 3.3-fold increases in ATPase activity, respectively), whereas the increase in ATPase activity for L464P reached a maximum of 5.8-fold at 800 nM p37 (Fig. 2C). We further investigated the binding of the Npl4-Ufd1 (NU) with p97 ATPase. Electron microscopic (EM) study demonstrated that the NU interacts with p97-NTD via the Npl4-UBX-L domain, which induces a conformational change for ATP hydrolysis [32, 34, 35, 50]. Our titration results identified the NU as an activator of $p97^{WT}$ ATP hydrolysis, starting at 20 nM and reaching a maximal 2.2-fold increase in activity at 200 nM, consistent with previously published studies (Fig. 2D) [49, 51]. Using the Walker B mutants of p97 (D1-E305Q and D2-E578Q) (Fig. S2B), we showed that D1-E305Q and $p97^{WT}$ have similar titration results. The result suggests that the NU activates D2 ATPase, because the D1 dead mutant (E305Q-p97) can hydrolyze ATP by the D2 ATPase, but not the D1 ATPase. The NU-mediated increases in ATPase activity (Fig. 2D) for linker mutants L464A and L464E were slightly less than the increases for $p97^{WT}$. The activation of the $p97^{L464P}$ mutant was 4.4-fold, about twice that of the $p97^{WT}$, and similar to the effect of p37. This supports that cofactor regulation by p37 and NU is affected by D1-D2 linker mutations to some extent.

Steady-state kinetic analysis of D1-D2 linker mutants and p97-cofactor complexes

To characterize the changes observed during the cofactor titrations, we measured the apparent steady-state kinetic constants for ATP hydrolysis for each enzyme-cofactor complex. The $p97^{L464P}$ mutant cofactor interactions produced the most significant changes in Michaelis-Menten (MM) curves (Fig. 3A). The apparent kinetic constants are summarized in Tables S1 and their ratio to without cofactor are shown in Table S3. The apparent maximum rate of ATP turnover (k_{cat}) for the $p97^{L464P}$ mutant was 3.3-fold lower than for $p97^{WT}$ (1.5 versus 4.7 min^{-1}) (Fig. 3B). However, the apparent Michaelis constant (K_m) for $p97^{L464P}$ did not differ substantially from the $p97^{WT}$ (Fig. 3C). Thus, the apparent overall catalytic efficiency (k_{cat}/K_m) of the $p97^{L464P}$ mutant was 3.8-fold lower than that of $p97^{WT}$, primarily due to the decreased rate of ATP hydrolysis (Fig. 3D). $p97^{L464A}$ and $p97^{L464E}$ mutants had apparent k_{cat}, apparent K_m, and apparent k_{cat}/K_m values within 2-fold of $p97^{WT}$ values (Fig. 3B-D).

p47 decreased the apparent ATP turnover number slightly for $p97^{WT}$ but increased the apparent k_{cat} for all three L464 mutants (Fig. 3B), most pronounced for $p97^{L464P}$ (3.3-fold; Fig. 3B) and comparable to levels for $p97^{WT}$ alone (5.0 min^{-1} vs. 4.7 min^{-1}, respectively). The apparent K_m values of $p97^{WT}$ and all three mutants, L464A, L464E and L464P, were all decreased by p47 compared to its basal ATPase activity without p47, supporting an interpretation that L464 mutations primarily affect p47-mediated changes in hydrolysis (apparent k_{cat}, in Fig. 3B) more than that of ATP binding (apparent K_m, in Fig. 3C). Compared to WT p97, the apparent K_m value is generally higher for the Linker mutants, thus the linker does affect ATP binding in the absent of p47. The presence of p47 rescued the defect of L464P in ATP hydrolysis (apparent k_{cat}) and made WT p97 and L464P similar. We previously demonstrated that p47 inhibits D2 ATPase hydrolysis, which requires active D1 hydrolysis [43]. Here, our results suggest that during p47 binding, L464 is required for the cross-inhibition of D1 on D2-driven ATP hydrolysis. Unlike p47, p37 and NU complexes produced similar steady-state kinetic profiles within 2-fold of $p97^{WT}$ values across the three mutants. This suggests that the distinct conformational changes that occur during p37 and NU binding were not significantly impaired by these L464 mutations. Thus, p97 control by p37 and NU differs from p47-mediated regulation.

Taken together, these findings indicate that the L464, located between the D1 and D2 domains (Fig. 1C), does not affect the apparent Michaelis constant (K_m) (Fig. 3C) but is instead critical for the hydrolysis steps of both basal and cofactor-regulated ATPase cycles of full-length p97. The $p97^{L464P}$ mutant had a 3.1-fold reduction in the k_{cat} for basal ATPase activity, which was rescued by all three cofactors, shown by increases in apparent k_{cat} of 3.3-fold (with p47), 6.0-fold (with p37), and 4.2-fold (with NU).

Elucidating the effect of linker mutants on D1 ATPase activity

Recently, NMR (nuclear magnetic resonance) spectroscopic analysis revealed that the WT-ND1L (residues 1-480 of p97) binding to monomeric p47 in solution with a Kd values of 230 nM determined by ITC [52]. The ND1L p97 protein is a robust, catalytically competent ATPase, similar to the D1 ATPase in full-length p97 [24]. Notably, ND1 proteins lacking the D1-D2 linker are enzymatically dead, indicating that the linker region is vital to D1 activity [24]. Therefore, ND1L can be used to scrutinize the D1-specific changes in ATPase kinetics for the linker mutants, with and without cofactor binding. Like the full-length version, L464E-ND1L exhibited basal ATPase activity (81.6%) comparable to activity for WT-ND1L. In contrast, L464P-ND1L retained only 1.7% of the activity of WT-ND1L (Fig. 4A), a level similar to that of ND1 (1.8% of WT-ND1L activity) [24]. The result suggests that introducing proline 464 into

ND1L significantly impairs the alignment of residues into the proper conformation so diminish the ability of D1 to hydrolyzing ATP as if the linker is completely removed. (Fig. 4A).

Size-exclusion chromatographic (SEC) profiles confirmed that the loss of activity in L464P-ND1L was not due to differences in the formation of proper oligomers, as compared to WT-ND1L. All three proteins had the same elution volume, and the oligomeric state of each was calculated to be 7.6 (Table S4). Based on published ND1 structures, we think ND1L is a hexamer; the calculated 7.6 oligomeric state for all of the ND1L proteins suggested their oligomeric state is the same. One crystal structure of p97 D2 domain showed a heptamer but the rest of p97 structures are all hexamers [53]. As with the full-length protein, dose-dependent cofactor titrations found differences in cofactor-regulated ATPase activity in wild-type ND1L versus ND1L mutants. In the presence of p47, the titration curves of WT-ND1L and L464E-ND1L remained flat, with activities close to baseline levels (Fig. 4B). However, L464P-ND1L had a dramatic 12-fold increase in ATPase activity at 800 nM p47, suggesting that the p47 binding to NTD causes a conformational change that alleviates the L464P defects in D1 hydrolysis.

We observed minor increases in the ATPase activity (1.3-fold) of the WT-ND1L with p37 (Fig. 4C), and a 3.7-fold increase for full-length $p97^{WT}$ (Fig. 2C), suggesting that p37 activation occurs primarily at D2 ATPase, consistent with previous data [43]. L464P-ND1L ATPase activity rose 4.7-fold with 800 nM p37. Heterodimer NU is an activator of full-length p97 (Fig. 2D). Yet, we found that NU inhibited hydrolysis in three ND1L proteins (Fig. 4D). For L464P-ND1L, we were unable to detect activity above background levels when using 25 nM monomer, due to the low basal activity of L464P-ND1L and the inhibitory effect of NU. We therefore increased the L464P-ND1L monomer concentration to 125 nM (5-fold) for NU titration. Still, we did not detect activity changes over 0.4 to 600 nM NU. At 800 nM (the equivalent of 160 nM NU per 25 nM L464P-ND1L monomer), we observed nearly 2-fold inhibition. WT-ND1L and L464E-ND1L variants followed similar titration curves, with inhibition starting at 60 nM, and about 2-fold decreases in ATPase activity at 200-800 nM NU (Fig. 4D).

To examine NU-mediated D1 and D2 ATPase activities in full-length p97, we used Walker B mutants, D1- E305Q and D2-E578Q, which allow ATP and ADP binding but block activation of hydrolysis. The NU titration curve for $p97^{WT}$ was similar to the curve for D1-305Q p97, whereas the D2-E578Q curve was relatively flat, with a small decrease (Fig. S2B). NU appears to inhibit D1 activity slightly while activating D2 activity in $p97^{WT}$. Comparison of titrations for ND1L (Fig. 4D) and D2-E578Q (Fig. S2B) suggest that NU inhibits D1 activity more when the D2 domain is absent.

Steady-state kinetic analysis of ND1L-domain mutants

The apparent steady-state kinetic constants of the ND1L proteins (Tables S2 and S3) with p47, p37 and NU were determined at 400 nM, the concentration that produced the maximum changes observed for wild type ND1L. Examples of MM curves for L464P-ND1L are shown in Fig. 5A. For WT-ND1L, only NU produced a >2-fold change in ATP turnover, reducing apparent k_{cat} values from 3.7 to 1.4 min^{-1} (Fig. 5B and Table S3). All three cofactors produced >2-fold decreases in apparent K_m values, indicating that they enhanced ATP binding specifically at the D1 domain (Fig. 5C). It appears that p37 and p47 enhance ATP binding to D1, thereby improving the apparent catalytic efficiency of D1 (k_{cat}/K_m). Intriguingly, NU increased the turnover number in full-length p97 but decreased the turnover number in ND1L, suggesting that NU specifically activates D2 catalysis.

L464E-ND1L and WT-ND1L displayed similar kinetic constants with all three cofactors (Figs. 5B-D), indicating that the hydrophobic nature of L464 is not a strict requirement for either basal ATPase activity or cofactor regulation at isolated D1 domains. In contrast, the L464P-ND1L dramatically reduced the apparent ATP turnover rate (k_{cat}) of D1 by 116-fold, from 3.7 to 0.032 min^{-1}, with no significant change in the K_m value. This observation suggests that the position 464 has structural requirements that are vital for D1 ATPase hydrolysis but not for ATP binding, consistent with previous comparisons of nucleotide-binding for ND1 versus ND1L [24].

In the presence of p47, L464P-ND1L apparent k_{cat} values (Fig. 5B) increased 14-fold, from 0.032 to 0.434 min^{-1}, without significant changes in apparent K_m. (Fig. 5C). It appears that binding to p47 primarily increases the catalytic ability of the L464P-ND1L protein, possibly through stabilization of the linker region that becomes distorted by the proline side chain. With p37, L464P-ND1L displayed a 7-fold increase in k_{cat} (Fig. 5B), and the apparent K_m value decreased 2.7-fold (Fig. 5C). This implies that p37, like p47, may also help stabilize the linker region. Cofactor complex NU inhibited L464P-ND1L to undetectable levels of ATPase activity across the measured ATP concentrations, similar to NU effects on WT-ND1L. Thus, we cannot report kinetic values for NU-regulated L464P-ND1L.

To summarize our results on full-length $p97^{WT}$ compared to ND1L: (1) p47 does not affect activity of ND1L but does regulate $p97^{WT}$ activity in a biphasic manner (Figs. 2B and 4B). (2) p47 decreases the apparent K_m of both ND1L and $p97^{WT}$ (Figs. 3C and 5C). (3) NU decreases ND1L activity while activating $p97^{WT}$ (Figs. 2D and 4D). (4) p37 caused a 1.5-fold increase in activity for ND1L (Fig. 4C) and a 4-fold increase for full-length p97 (Fig. 2C), which supports an earlier finding that p37 mainly activates D2 [43]. Overall, these results suggest that the mechanisms by which cofactors regulate D1 and full-length p97 (D1 and D2) differ, with distinct mechanisms for each cofactor.

L464P reduced p47 binding to full length p97 but not to the ND1L truncated mutant

Two evaluate whether changing the conserved L464 to E or P will affect p47 binding, we used temperature-related intensity change (TRIC) on a DianthusNT.23 PicoDuo instrument to determine the equilibrium binding constant (K_d) for p47 in solution with six p97 proteins (Fig. S3). The K_d values are 80, 182, 376 nM for $p97^{WT}$, $p97^{L464E}$, and $p97^{L464P}$, respectively. These results suggested a 4.7-fold reduction of p47 binding affinity caused by proline for full length p97. The K_d values are 343, 264, 271 nM for WT-ND1L, L464E-ND1L, and L464P-ND1L, respectively. These results suggested a 4.3-fold reduction of p47 binding affinity for ND1L as compared to full length p97 and the binding affinity of L464P-ND1L is similar to WT-ND1L.

Structure of the full-length $p97^{L464P}$ reveals conformational changes caused by changing the conserved L464 at the D1-D2 linker

We showed that L464 is the key residue on the D1-D2 linker for modulating p97 ATPase function, we want to determine whether the L464 mutation alters the D1-D2 linker conformation, thereby affecting the ATPase activity. We utilized single-particle cryo-EM imaging to determine the three-dimensional (3D) structure of the $p97^{L464P}$ (Fig. S4 and S5). The cryo-EM reconstruction of the $p97^{L464P}$ showed the same hexameric organization as the wild type p97, suggesting that the L464P mutation does not affect the p97 oligomerization (Fig. S4A and 6A). The cryo-EM reconstruction showed four clear NTD densities in the down conformation, with two NTDs in lower signal levels (Fig. 6A). The density maps allowed us to dock the p97 coordinates (Fig. S5). The resolved NTDs are all in the down configuration,

implying less mobility than the others (Fig. 6A). The unresolved mobile NTD densities may be due to their high flexibility, resulting in density flattening. Unlike the homogeneous NTD configuration in the wild type [25], the highly flexible NTDs of the $p97^{L464P}$ could be due to the linker mutation and the altered communication between domains, resulting in undefined positions of the NTDs in cryo-EM density maps.

Unlike the NTD densities, the D1 and D2 densities were well resolved in our cryo-EM reconstructions. To visualize the details of the structural changes between domains, we then attempted to average six D1 and D2 densities symmetrically (Fig. S6). We further superimposed our structure with $p97^{WT}$ (PDB code: 5FTK) (RMSD 1.162 Å) (Fig. 6B). The D1-D2 linker changes its structure upon L464P mutation, which causes a slight movement of the helix-turn-helix (HTH) motif of K543-A569 (Fig. 6C and D). Also, the loop densities (K584-D598) for the D2 ring in the L464P mutant were missing, suggesting a flexible nature and size variation of the D2 ring. These local structural changes could be attributed to the change of the loop torsion contributed from the geometric constraints of proline residue (Fig. 6C and D). The structural changes of the HTH motif and D2 ring could affect the concerted movement between protomers and thereby the ATPase activities.

L464 mutation decreases the potency of p97 inhibitors

Because p97 plays a vital role in protein quality control, much has been done in recent years to target p97 with potent and specific inhibitors for potential cancer therapy [16, 54-56]. These compounds are divided into two major classes: ATP-competitive inhibitors [57, 58] and noncompetitive inhibitors [59-61]. We previously evaluated the domain and cofactor-complex selectivity of these compounds, finding that communication between the D1 and D2 domains changes the ability of each inhibitor to affect ATPase activity [24, 51, 62]. For example, mutations within the ND1 domain can significantly increase the IC_{50} of the D2-specific inhibitor ML240 [24]. In addition, the allosteric p97 inhibitor NMS-873 binds in a cavity formed by the D1 and D2 regions of the hexamer in close proximity to L464 and $p97^{L464E}$ is 2-fold less sensitive to NMS-873 [59]. Furthermore, we established that CB-5083-resistant ovarian cancer cells carried E470K and E470D missense mutants that lead to increased p97 ATPase activity [63]. Therefore, we want to test if L464 mutants might affect the potency of the ATP-competitive p97 inhibitors.

To examine inhibitor potency in relation to L464 mutations, we determined IC_{50} values for four ATP-competitive inhibitors we previously identified -- DBeQ, ML240, ML241, CB-5083) [57, 58] and the non-competitive inhibitor (NMS-873) [59] -- against each of the L464 mutants and $p97^{WT}$ (Fig. 7). Structures of p97 inhibitors are shown in Figure 7A. The allosteric inhibitor NMS-873, which binds close to the D1-D2 linker, had a 2.6-fold increase in the IC_{50} value for the L464E mutant (Fig. 7B). The result corroborates previously published data [59]. The L464A and L464P mutants did not significantly affect the IC_{50} values for NMS-873, which suggested that NMS-873 could still bind to these two mutants.

The ATP-competitive inhibitor DBeQ, which inhibits both D1 and D2 ATPase activities, was not affected by L464 mutations, showing similar potencies towards the three linker mutants and $p97^{WT}$ (Fig. 7C). On the other hand, the D2-specific inhibitors, ML240, ML241, and CB-5083, had 2 to 3-fold increases in IC_{50} values for the L464 mutants (Figs. 7D and 7E). Interestingly, the IC_{50} increased is more for ML240 than that of CB-5083, which is consistent with the finding for E470K and E470D mutants [63]. Because the L464 resides in the D1-D2 linker region and because the mutations reduced the effects of the D2-binding inhibitors, the

experiment further supports the conclusion that altering L464 can impair either the D2 conformation or communication between the D1 and D2 domains, to hinder the binding of D2-specific inhibitors.

Discussion

As an AAA+ ATPase protein, p97 acts as the primary molecular machine in several cellular processes vital to protein homeostasis and cell survival. Over the past several decades, structural analyses and biochemical assays on p97 have identified many essential and conserved regions. Mutations in these regions result in cell-based defects and/or ATPase activity defects. Several p97 cofactors are thought to direct p97 to various cellular functions via discrete and/or overlapping binding sites in the NTD or the C-terminal tails [28, 64, 65]. Cofactor binding results in a conformational change of p97, leading to modulation of the enzyme kinetics of ATP hydrolysis [66]. Previous studies suggest that p97 disease mutants cause imbalanced cofactor binding such as Npl4-Ufd1 but not p47 impairs binding of UBE4B to p97 [67] and also impairs UBXD1 binding to p97 [68]. A better understanding of these cofactor-regulated changes is imperative for increased knowledge of disease pathogenesis and for providing valuable insight into possible therapeutic approaches.

We explored the role of cofactor-mediated p97 regulation in IBMPFD, a rare disease characterized by large cellular inclusion bodies, indicative of possible defects in the p97 protein degradation pathways [43]. Several disease-causing variants have been biochemically characterized and found to raise basal levels of ATPase activity. Therefore, ATPase activity alone is not the sole indicator of an efficient, functional p97 protein. We found that three disease-causing p97 mutations display altered cofactor regulation. Specifically, the D2 domain of IBMPFD mutants could not be activated by either p37 or p47. This suggests that these defects may contribute to the pathogenesis of the disease. We also identified amino acids 69 to 92 of p47 as responsible for the observed difference for p37 and p47 in regulating p97 ATPase activity [43]. The binding modes of the two cofactors are highly similar and it is possible that upon binding to p97 the amino acids 69 to 92 of p47 induce conformational changes to case inhibition of both D1 and D2 domain at lower concentration of p47. Without this region p37 cannot cause such inhibition. Recently, the role of two related p97 cofactors, p47 and p37, in protein phosphatase 1 (PP1) maturation revealed an interesting ubiquitin-independent unfolding function to regulated PP1 complex disassembly and assembly [69].

Here we have demonstrated that the Npl4-Ufd1 heterodimer is an activator of the D2 domain and an inhibitor of the D1 domain of the $p97^{WT}$ (Fig. 2D and 4D). This supports the validity of studying cofactor-regulated p97 activity. The Npl4-Ufd1 heterodimer binds via the ubiquitin-like (UBX-L) domain of Npl4, similar to the p47-UBX domain. The binding of the two cofactors is mutually exclusive, suggesting that they either bind at the same site or prevent the other from binding [70]. The increase in ATPase activity observed for NU may also be involved in coordinating and accelerating its function in the ERAD pathway. Tang and Xia showed that the N-terminal half of the D1-D2 linker is essential for the activity of the D1 domain. By comparing the X-ray crystal structures of the isolated D1 domain with and without the D1-D2 linker, they showed that the linker region is required to break the symmetric arrangement of the D1 ring and enable ATP hydrolysis [23, 42]. Bastola and coauthors reported a potentially direct effect of the E470 mutations on the interactions between the ligand and target [63]. Here, we pinpoint the critical role of the conserved L464 residue in the D1-D2 linker region of

p97 by studying the enzymatic activity of point mutants of L464 in both full-length p97 and the isolated D1 domain.

We showed that the L464P mutation reduced by 51% the activity of full-length $p97^{WT}$ (in which both the D1 and D2 domains are active ATPases; Figs. 2A and 8A). Consistent with the published data on $p97^{L464E}$ [39], both $p97^{L464A}$ (with a smaller side chain) and $p97^{L464E}$ (with a negatively charged side chain) retained 100% of $p97^{WT}$ activity. However, the L464P mutation disrupted the activity of $p97^{WT}$, possibly due to the proline side chain caused conformational change (Fig. 6). To evaluate the effect of L464P specifically on D1 activity, we made an L464P-ND1L protein (which has an active D1 domain with the linker) and showed that L464P diminished ND1L activity to the levels found for deletion of the entire linker (Figs. 4A and 8B). The results suggest that the structural flexibility of L464 in the D1-D2 linker is important for the basal activity of $p97^{WT}$. The severe effect of the proline mutation on the isolated D1 domain (L464P-ND1L) indicates that the proper structure of the D1-D2 linker is vital to D1 function. Due to the proximity of L464 to the nucleotide-binding pocket of the D1 domain (Fig.1B), it is possible that its flexibility is required for the overall movement that occurs during ATP hydrolysis, but not ATP binding. This interpretation is supported by the fact that the apparent K_m value of L464P-ND1L does not differ from the apparent K_m value of WT-ND1L (Fig. 5C), but the apparent k_{cat} value of L464P-ND1L is 115-fold lower than the WT-ND1L value (Table S2).

Although the basal ATPase activities of $p97^{L464A}$ and $p97^{L464E}$ are similar to that of the $p97^{WT}$, the mutations caused severe defects in the clearance of the ERAD substrate TCR-α-GFP [39] and the UFD pathway reporter (Ub^{G76V}-GFP) (Fig. S1). Here we showed that the cellular defects observed with the L464 mutants may be due to abnormal cofactor-regulated p97 enzyme function. The L464 mutants and the full-length $p97^{WT}$ displayed similar basal steady-state kinetics, but the mutants had a complete loss of p47-regulated inhibition (Figs. 2-3). Instead, p47 had only single-phase activation with the mutants, which appeared to enhance the phase 2 rebound normally observed with the $p97^{WT}$. L464P-p97 had much greater activation, compared to the more flexible alanine and glutamate mutants, for the three cofactors tested (Figs. 2B-D). Furthermore, $p97^{L464A}$ and $p97^{L464E}$ actually reduced activation by p37 (Fig. 2C) and NU (Fig. 2D), whereas L464P enhanced activation of full-length p97 by both p37 and NU. These three-point mutations in the D1-D2 linker region clearly altered cofactor-regulated p97 ATPase activities.

Previous structural studies on p97 and yeast homolog Cdc48 have provided valuable insight on this versatile ATPase [52, 71-73]. $p97^{WT}$ is highly dynamic upon cofactor binding, and some mutation sites were found to stabilize the complex; for example, $p97^{A232E,E578Q}$ double mutations were introduced in Pan et. al [37]. NMR study suggested that an intrinsically disordered region regulates the interaction between p47 and the truncated p97-ND1L [52]. Shp1, a yeast p47 homolog, was used to pull down Cdc48 in the presence of nonhydrolyzable ATP analog with an endogenous polypeptide. The cryo-EM analysis of this complex implied a hand-over-hand mechanism of substrate translocation of the AAA+ ATPase [74]. Using $Cdc48^{E588Q}$, a D2 ATPase-dead mutant complex with Npl4-Ufd1 can pull a ubiquitinylated substrate through the central pore [75].

Blythe et. al showed that in the presence of ATP, $p97^{WT}$ has 50% up and down NTD and the NTDs of the $p97^{A232E}$ are all in up position [36]. In the presence of ADP, all resolved $p97^{WT}$ NTD showed down positions and $p97^{A232E}$ show more than 50% mobile NTD and 20% visible down position and less than 10% up position [26]. In our $p97^{L464P}$ structure, we did not supply any nucleotides and we observed four clear NTD densities in the down conformation

and two NTDs in lower signal levels (Fig. 6A). Our results indicate that the resolved NTDs in the $p97^{L464P}$ resemble the NTDs in the ADP-bound $p97^{WT}$.

Recently, Pan and coauthors solved several cryo-EM structures of p97A232E, E578Q with Npl4-Ufd1; they used the mutant A232E to lock N-domain in a more up-conformation and E578Q to block D2 ATP hydrolysis to enable a stable complex with Npl4/Ufd1 and polyubiquitinated substrate, and they observed conformational change at L464 amino acid by comparing the ATPγS-bound non-translocating structure with the ATPγS-bound plus substrate (PDB ID: 7JY5) [37, 76]. By comparing two ATPγS-bound p97 structures, with and without substrate, they demonstrated L464A has reduced unfoldase activity using the polyubiquitinated substrate [76]. In vitro study using artificial mutant such as E578Q to abolish ATP hydrolysis is one of the methods to enable visualization of the dynamic p97 protein. Similarly, even though ATPase activity alone is not the sole indicator of p97 function, it does provide direct evidence of how a single amino acid change can change it basal and cofactor-regulated ATPase activities. We think the difference in cofactor-regulated ATPase activity can potentially indicate difference in regulating p97's endogenous substrates associated with a specific cofactor, but this remains to be determined.

In recent years, an upsurge in p97 inhibitor development has yielded promising starting points for future therapies. A number of structure-activity relationship studies have been aimed towards tailoring inhibitors to specific p97 functions [49, 51, 60-62, 77]. We found that L464 is critical for determining the functionality of p97 inhibitors. Specifically, mutating L464 diminished by 3-fold the inhibitory effects of D2 ATP-competitive inhibitors, ML240 and ML241 (Fig. 7D and E). We reconfirmed findings that an L464 mutant reduced the potency of NMS-873 (Fig. 7B), an inhibitor that binds in the linker region [59]. From these results, we conclude that L464 is critical for maintaining the correct conformation of the linker region, and that disturbing the conformation of the linker can impact how D2-selective ATP competitive inhibitors bind to the D2 ATPase domain.

Our model suggests that the conserved L464 in the D1-D2 linker (22 amino acids, Fig. 8) is necessary to maintain communication among the domains of p97, including NTD, D1, and D2, regardless of their distances from one another in space. The L464P mutation changes the conformation of the linker region, lowering the efficiency of ATP hydrolysis by reducing ATPase activities (Fig. 8A). For the isolated D1 domain with the linker (ND1L), the L464P mutation induces a conformational change that nearly abolishes its ability to hydrolyze ATP (Fig. 8B). The L464P-ND1L is enzymatically comparable to the ND1 protein, which lacks the linker region entirely [24]. This substantial loss of activity compared to WT-ND1L demonstrates the importance of the linker region for D1 ATPase function, a finding consistent with our previous results [24]. In addition, we propose that although the L464P mutation alters the conformation of the p97 D1-D2 linker, the presence of p47 restores the conformation to some degree, through stabilization of the linker region of L464P (Fig. 8B). This interpretation would explain why p47 has no appreciable effect on WT-ND1L ATPase activity, but activates the L464P-ND1L mutant by 12-fold (Fig. 5B and 8B).

This study adds to our growing understanding of p97 and its function. We have determined that the conformation of the linker region is crucial to ATP hydrolysis at the D1 and D2 domains. We identified the importance of these regions in communication within the enzyme during cofactor-regulated ATPase activity and demonstrated that three p97 cofactors regulate the enzyme differently. Even though the total p97 protein level is more than individual

p97 cofactors but published result suggests that in normal condition, most p97 cofactors are not associated with p97 and the association can be enhanced under some conditions. For example, Xue and coauthors used size exclusion chromatography to separate cellular p97 and p97 cofactor complexes in HEK293 coupled with mass spectrometry to infer that the cofactors interaction with p97 are very dynamic; they also found p47 and Npl4-Ufd1 do not cofractionate with p97 in unperturbed cell lysate and upon p97 inhibition by an allosteric inhibitor NMS-873 enhanced formation of the complexes, but most of cofactors are still not associated with p97 [78]. Therefore, future studies of the remaining known UBX cofactors are warranted. Additionally, comprehensive structural data of p97 cofactors are not available. For example, even though p47 has been studied with great interest since its discovery in 1997 [29] and the structures of p47 revealed that conformational changes in p97 are induced [29, 79, 80]. Structural data for p97 bound with the full-length p47 and other p97 cofactors would provide evidence for the conformational changes resulting from cofactor interaction. In addition, it is likely that the p97 function is modulated by its substrates, as well as its cofactors. Future work should examine the role that endogenous substrates play in cofactor-regulated p97 activity. Given our knowledge gained from more thoroughly studying the enzyme-cofactor relationship, it is reasonable to infer that each p97 enzyme-cofactor complex is fine-tuned for the microenvironment where it performs its role. Therefore, a better understanding of these complexes will yield valuable insights into the biochemical intricacies of their functions. We believe that our research provides new information useful for understanding how p97 cofactors regulate p97 function and for developing p97-specific therapeutic agents.

Materials and Methods

Ubiquitin fusion degradation pathway reporter assay. The HeLa cells that stably expressed Ub^{G76V}-GFP are described previously [46,48]. Cells were treated with TrypLE Select (Thermo Fisher) and counted the day before transfection. Cells were then plated, 3000 cells per well, in 30uL of 10% FBS clear growth medium. Cells were observed to be 80-90% confluent the day of transfection. Transfection complexes for each sample were prepared by mixing 2 µg of DNA, 3uL of BioT reagent (Bioland Sci), and 100 µL of Serum-free DMEM, and incubating for 25 minutes at 25°C. 10 µL of the DNA-BioT complexes were then added directly to each well containing cells and mixed on a rocker. Plates were incubated at 37°C in a CO_2 incubator for 24 hours, then read using ImageXpress (Molecular Device).

Preparation of p97 ATPase proteins. Plasmids used for generating p97 and ND1L proteins can be found in supplemental Table S6. Proteins were purified as previously described [24, 57].

Determining IC_{50} values of p97 inhibitors in ATPase assays. The detailed method was described previously [24]. Inhibition of human p97 (25 nM monomer) was carried out in assay buffer (50 mM Tris (pH 7.4), 20 mM $MgCl_2$, 1 mM EDTA and 0.5 mM TCEP) containing 0.01% Triton X-100 and 200 µM ATP. The 8-dose titration was performed at 40, 13.3, 4.4, 1.48, 0.49, 0.16, 0.05, and 0 µM. ATPase activity was determined through the addition of Biomol Green Reagent (Enzo Life Sciences). NMS-873 was purchased from Xcess Biosciences Inc.

Gel filtration to confirm the stability of the mutant p97 and p47 complex. Gel filtration was carried out with a Superdex 200 10/300 GL (GE Healthcare). The column was calibrated with molecular weight (MW) standards kit (Sigma). The standards are Blue Dextran [MW is 2000 kDa; used to determine the void volume (*V*o) of the column], β-amylase (200 kDa), alcohol dehydrogenase (150 kDa), bovine serum albumin (66 kDa), and carbonic anhydrase (29 kDa). The linear molecular weight calibration plotted Ve/Vo versus Log MW (see standard curve),

where *V*e is the elution volume of the MW standard and Vo is the void volume. To determine the apparent molecular weight of WT-ND1L, L464E-ND1L, and L464P-ND1L, we injected 100 μL of 20 μM proteins, determined their elution volumes (*V*e), and then calculated apparent molecular weights using the equation obtained from the standard curve. The calculated MW was divided by the monomer MW to calculate the oligomeric state.

Cryo-EM data collection and image analysis. For $p97^{L464P}$ mutant, a holey-carbon C-flat grid (2/1 4C; Protochips, Morrisville, NC) was glow-discharged for 15 seconds using a Pelco easiGlow glow-discharge system (Ted Pella, Redding, CA). 6 μL protein sample at a concentration of 0.2 mg/mL was applied onto the pretreated grid, and the excess solution was blotted away by a filter paper (Whatmann 55/20 nm) using a Thermo Fisher/FEI Vitrobot Mark IV automated freeze plunger (Thermo Fisher/FEI, Hillsborough, OR) for 6 seconds in a chamber with a humidity of 100%. The grid was then quickly plunged frozen into liquid ethane and transferred to a grid storage. Particle homogeneity and ice thickness of the grid specimen were screened using a FEI Tecnai TF20 TEM. Grids with a thin ice and a homogeneous protein dispersion were used for the subsequent cryo-EM data collection.

The grid specimen was imaged using a Thermo Fisher/FEI Titan Krios TEM at an accelerating voltage of 300 keV at the Eyring Materials Center (EMC) at Arizona State University (ASU), Tempe, AZ. Cryo-EM movies were recorded using a Gatan K2 Summit direct electron detector (DED) camera (Gatan, Pleasanton, CA). Defocus range was set to -0.8 to -2.5 μm. Nominal magnification was 48,077×, resulting in a physical pixel size of 1.04 Å/pixel at the specimen level. The movie data was recorded at a counted rate of 8.096 e^-/pixel/sec and a sub-frame rate of 200 msec in counting mode. Total exposure was 8 seconds, accumulating to a dosage of 64.8 $e^-/Å^2$. Beam-image shift was applied to accelerate the data acquisition [81]. The data collection was automated using the customized SerialEM macros (version 3.9) [82].

The image processing for the $p97^{L464P}$ dataset was generally conducted using cryoSPARC software (version 3.1) [83]. 4,490 movies were unpacked and imported into cryoSPARC program. The frame registration and averaging were performed using patch motion correction. The defocus parameters were estimated using patch CTF estimation. The particle selection was performed using Topaz program (version 0.2.3) [84]. The two-dimensional (2D) unsupervised classification was performed to generate the averages from the selected particle pool. The classes with discernible features were selected for *ab initio* volume generation using stochastic gradient descent (SGD) method [83]. Further particle image curation was performed using 2D image classification, *ab initio* 3D generation supplied with a higher *k* value and heterogeneous refinement. The final 3D density was then refined against the experimental images using homogeneous refinement and non-uniform refinement [85]. The generated maps reached final resolutions of 5.16 Å. The final resolution of the density map was determined using the golden FSC criteria at 0.143 cutoff [86]. To visualize the details of the D1 and D2 domains, the densities of the D1 and D2 domains were symmetrically averaged supplied with a local mask only containing D1 and D2 domains. The resolution of the symmetrically averaged density reaches 4.12 Å. The processing schematics and data statistics are shown in Fig. S4 and Table S6.

Modeling. The templates used for atomic modeling were the previous coordinates of p97 (PDB code: 5FTK) [25]. The templates were first docked into individual cryo-EM densities using 'Fit in the Map' function in UCSF Chimera (version 1.14) [87]. The fitted model was manually rebuilt using Coot (version 0.9.4) [88] and then refined against the cryo-EM densities using

'phenix.real_space_refine' program in Phenix software package (version 1.18.2-3874) [89]. Hydrogen atoms were added using 'phenix.reduce' for the model refinement and removed after the refinement. Secondary structure restraints were applied during the model refinement. The refinement and validation statistics was listed in Table S6. The figures for the cryo-EM density maps and atomic models were prepared using UCSF Chimera or ChimeraX (version 1.0) [90].

*BIOMOL Green ATPase assay***.** Detection of ATPase activity using BIOMOL Green reagent (Enzo Life Sciences) was performed as previously described [43]. Purified p97 or ND1L proteins (25 μL of 50 μM; final concentration = 25 nM monomer concentration) were used with 400 nM cofactor proteins. For generating Michaelis-Menten (MM) curves, at least 8 concentrations of ATP were utilized in at least 6 replicate reactions, and all calculations were made using GraphPad Prism 7.0 by fitting data to Equation 1.

$$v = V_{max}\cdot[ATP]/(K_m + [ATP]) \quad \textbf{(1)}.$$

Molecular graphics. The figure of the p97 structures was prepared using UCSF ChimeraX [90] with the atomic coordinates from the PDB codes of 5TFN (down) [77], 5TFM (up) [77], and 1S3S ($p97^{N\text{-}D1}$-$p47^{UBX}$) [71].

p47 binding affinity measurements. The binding affinity (K_d values) between p47 and $p97^{WT}$ or p97 mutants was determined by measuring the temperature-related intensity change (TRIC) signals using a Dianthus NT.23 instrument (Nano-Temper Technologies, München, Germany). p47 was labeled with a RED-NHS dye using the Monolith Protein Labeling Kit RED-NHS second-generation (Nano-Temper Technologies, CAT# LO-L011). Full-length wild type or mutant p97 was titrated against 10 nM of p47-NHS in two-fold steps from 2.8 μM to 1.37 nM in 20 μL working buffer (20 mM HEPES (pH 7.4), 150 mM KCl, 1 mM $MgCl_2$, 5% (w/v) glycerol, and 0.0025% (v/v) Tween 20). Assays were performed in a Dianthus 384-well plate in three independent experiments. Data from three independent measurements were fitted using non-linear regression analysis in Prism 7.0.

Data availability. Cryo-EM density maps were deposited in the Electron Microscopy Data Bank (EMDB) under accession numbers of EMD-23775 and EMD-23776 (symmetrized) and the Protein Data Bank (PDB) under accession numbers of 7MDM and 7MDO (symmetrized). All data are available from the corresponding author upon request.

Acknowledgements

Cryo-EM data collection was by the use of the Titan Krios TEM at the Eyring Materials Center at Arizona State University, with funding for the instrumentation by NSF MRI 1531991. Special thanks to Dewight Williams for assisting cryo-EM data collection. Computation for image processing was partly supported by the NVIDIA GPU Grant Program. Molecular graphics and analyses performed with the UCSF ChimeraX was supported by NIH R01-GM129325 and the Office of Cyber Infrastructure and Computational Biology, NIAID. This project was supported in part with funds from the National Institute of Neurological Disorders and Stroke, R01NS100815 and R01NS102279.

Author contributions

XZ, LG, SL, PN, PLC, TFC designed the research. XZ, LG, SL, PN, RCC, DEW and DRM performed the research. LG, XZ, SL, PN, DEW, DRM, HJL, PLC and TFC analyzed the data and composed the paper.

Financial Disclosure

The authors have no competing financial interests to disclose.

References

[1] Boyault C, Zhang Y, Fritah S, Caron C, Gilquin B, Kwon SH, et al. HDAC6 controls major cell response pathways to cytotoxic accumulation of protein aggregates. Genes Dev. 2007;21:2172-81.
[2] Golbik R, Lupas AN, Koretke KK, Baumeister W, Peters J. The Janus face of the archaeal Cdc48/p97 homologue VAT: protein folding versus unfolding. Biol Chem. 1999;380:1049-62.
[3] Ju JS, Miller SE, Hanson PI, Weihl CC. Impaired protein aggregate handling and clearance underlie the pathogenesis of p97/VCP-associated disease. J Biol Chem. 2008;283:30289-99.
[4] Wolf DH, Stolz A. The Cdc48 machine in endoplasmic reticulum associated protein degradation. Biochim Biophys Acta. 2012;1823:117-24.
[5] Cao K, Nakajima R, Meyer HH, Zheng Y. The AAA-ATPase Cdc48/p97 regulates spindle disassembly at the end of mitosis. Cell. 2003;115:355-67.
[6] Meyer H, Bug M, Bremer S. Emerging functions of the VCP/p97 AAA-ATPase in the ubiquitin system. Nat Cell Biol. 2012;14:117-23.
[7] Richly H, Rape M, Braun S, Rumpf S, Hoege C, Jentsch S. A series of ubiquitin binding factors connects CDC48/p97 to substrate multiubiquitylation and proteasomal targeting. Cell. 2005;120:73-84.
[8] Bonizec M, Herissant L, Pokrzywa W, Geng F, Wenzel S, Howard GC, et al. The ubiquitin-selective chaperone Cdc48/p97 associates with Ubx3 to modulate monoubiquitylation of histone H2B. Nucleic Acids Res. 2014;42:10975-86.
[9] Dantuma NP, Acs K, Luijsterburg MS. Should I stay or should I go: VCP/p97-mediated chromatin extraction in the DNA damage response. Exp Cell Res. 2014;329:9-17.
[10] Tresse E, Salomons FA, Vesa J, Bott LC, Kimonis V, Yao TP, et al. VCP/p97 is essential for maturation of ubiquitin-containing autophagosomes and this function is impaired by mutations that cause IBMPFD. Autophagy. 2010;6:217-27.
[11] Dargemont C, Ossareh-Nazari B. Cdc48/p97, a key actor in the interplay between autophagy and ubiquitin/proteasome catabolic pathways. Biochim Biophys Acta. 2012;1823:138-44.
[12] Bug M, Meyer H. Expanding into new markets--VCP/p97 in endocytosis and autophagy. J Struct Biol. 2012;179:78-82.
[13] Hill SM, Wrobel L, Ashkenazi A, Fernandez-Estevez M, Tan K, Burli RW, et al. VCP/p97 regulates Beclin-1-dependent autophagy initiation. Nat Chem Biol. 2021;17:448-55.
[14] Fessart D, Marza E, Taouji S, Delom F, Chevet E. P97/CDC-48: proteostasis control in tumor cell biology. Cancer Lett. 2013;337:26-34.
[15] Stolz A, Hilt W, Buchberger A, Wolf DH. Cdc48: a power machine in protein degradation. Trends Biochem Sci. 2011;36:515-23.
[16] Deshaies RJ. Proteotoxic crisis, the ubiquitin-proteasome system, and cancer therapy. BMC Biol. 2014;12:94.
[17] Kakizuka A. Roles of VCP in human neurodegenerative disorders. Biochem Soc Trans. 2008;36:105-8.
[18] Koppers M, van Blitterswijk MM, Vlam L, Rowicka PA, van Vught PW, Groen EJ, et al. VCP mutations in familial and sporadic amyotrophic lateral sclerosis. Neurobiol Aging. 2012;33:837 e7-13.
[19] Johnson JO, Mandrioli J, Benatar M, Abramzon Y, Van Deerlin VM, Trojanowski JQ, et al. Exome sequencing reveals VCP mutations as a cause of familial ALS. Neuron. 2010;68:857-64.
[20] Guinto JB, Ritson GP, Taylor JP, Forman MS. Valosin-containing protein and the pathogenesis of frontotemporal dementia associated with inclusion body myopathy. Acta Neuropathol. 2007;114:55-61.
[21] Clemen CS, Winter L, Strucksberg KH, Berwanger C, Turk M, Kornblum C, et al. The heterozygous R155C VCP mutation: Toxic in humans! Harmless in mice? Biochemical and biophysical research communications. 2018;503:2770-7.
[22] Wang Q, Song C, Yang X, Li CC. D1 ring is stable and nucleotide-independent, whereas D2 ring undergoes major conformational changes during the ATPase cycle of p97-VCP. J Biol Chem. 2003;278:32784-93.
[23] Xia D, Tang WK, Ye Y. Structure and function of the AAA+ ATPase p97/Cdc48p. Gene. 2016;583:64-77.
[24] Chou TF, Bulfer SL, Weihl CC, Li K, Lis LG, Walters MA, et al. Specific inhibition of p97/VCP ATPase and kinetic analysis demonstrate interaction between D1 and D2 ATPase domains. J Mol Biol. 2014;426:2886-99.
[25] Banerjee S, Bartesaghi A, Merk A, Rao P, Bulfer SL, Yan Y, et al. 2.3 Å resolution cryo-EM structure of human p97 and mechanism of allosteric inhibition. Science. 2016;351:871-5.
[26] Blythe EE, Gates SN, Deshaies RJ, Martin A. Multisystem Proteinopathy Mutations in VCP/p97 Increase NPLOC4.UFD1L Binding and Substrate Processing. Structure. 2019;27:1820-9 e4.
[27] Schuberth C, Buchberger A. UBX domain proteins: major regulators of the AAA ATPase Cdc48/p97. Cell Mol Life Sci. 2008;65:2360-71.
[28] Yeung HO, Kloppsteck P, Niwa H, Isaacson RL, Matthews S, Zhang X, et al. Insights into adaptor binding to the AAA protein p97. Biochem Soc Trans. 2008;36:62-7.

[29] Kondo H, Rabouille C, Newman R, Levine TP, Pappin D, Freemont P, et al. p47 is a cofactor for p97-mediated membrane fusion. Nature. 1997;388:75-8.
[30] Kaneko Y, Shimoda K, Ayala R, Goto Y, Panico S, Zhang X, et al. p97 and p47 function in membrane tethering in cooperation with FTCD during mitotic Golgi reassembly. EMBO J. 2021:e105853.
[31] Uchiyama K, Totsukawa G, Puhka M, Kaneko Y, Jokitalo E, Dreveny I, et al. p37 is a p97 adaptor required for Golgi and ER biogenesis in interphase and at the end of mitosis. Developmental cell. 2006;11:803-16.
[32] Bodnar NO, Kim KH, Ji Z, Wales TE, Svetlov V, Nudler E, et al. Structure of the Cdc48 ATPase with its ubiquitin-binding cofactor Ufd1-Npl4. Nature structural & molecular biology. 2018;25:616-22.
[33] Hanzelmann P, Schindelin H. Characterization of an Additional Binding Surface on the p97 N-Terminal Domain Involved in Bipartite Cofactor Interactions. Structure. 2016;24:140-7.
[34] Bebeacua C, Forster A, McKeown C, Meyer HH, Zhang X, Freemont PS. Distinct conformations of the protein complex p97-Ufd1-Npl4 revealed by electron cryomicroscopy. Proceedings of the National Academy of Sciences of the United States of America. 2012;109:1098-103.
[35] Isaacson RL, Pye VE, Simpson P, Meyer HH, Zhang X, Freemont PS, et al. Detailed structural insights into the p97-Npl4-Ufd1 interface. J Biol Chem. 2007;282:21361-9.
[36] Blythe EE, Olson KC, Chau V, Deshaies RJ. Ubiquitin- and ATP-dependent unfoldase activity of P97/VCP*NPLOC4*UFD1L is enhanced by a mutation that causes multisystem proteinopathy. Proceedings of the National Academy of Sciences of the United States of America. 2017;114:E4380-E8.
[37] Pan M, Zheng Q, Yu Y, Ai H, Xie Y, Zeng X, et al. Seesaw conformations of Npl4 in the human p97 complex and the inhibitory mechanism of a disulfiram derivative. Nat Commun. 2021;12:121.
[38] Liu CC, Sun S, Sui SF. The role of the N-D1 linker of the N-ethylmaleimide-sensitive factor in the SNARE disassembly. PLoS One. 2013;8:e64346.
[39] Li G, Huang C, Zhao G, Lennarz WJ. Interprotomer motion-transmission mechanism for the hexameric AAA ATPase p97. Proceedings of the National Academy of Sciences of the United States of America. 2012;109:3737-41.
[40] Huang C, Li G, Lennarz WJ. Dynamic flexibility of the ATPase p97 is important for its interprotomer motion transmission. Proceedings of the National Academy of Sciences of the United States of America. 2012;109:9792-7.
[41] Wang Q, Song C, Irizarry L, Dai R, Zhang X, Li CC. Multifunctional roles of the conserved Arg residues in the second region of homology of p97/valosin-containing protein. J Biol Chem. 2005;280:40515-23.
[42] Tang WK, Xia D. Role of the D1-D2 Linker of Human VCP/p97 in the Asymmetry and ATPase Activity of the D1-domain. Sci Rep. 2016;6:20037.
[43] Zhang X, Gui L, Zhang X, Bulfer SL, Sanghez V, Wong DE, et al. Altered cofactor regulation with disease-associated p97/VCP mutations. Proceedings of the National Academy of Sciences of the United States of America. 2015;112:E1705-14.
[44] Bulfer SL, Chou TF, Arkin MR. p97 Disease Mutations Modulate Nucleotide-Induced Conformation to Alter Protein-Protein Interactions. ACS chemical biology. 2016;11:2112-6.
[45] Erzurumlu Y, Kose FA, Gozen O, Gozuacik D, Toth EA, Ballar P. A unique IBMPFD-related P97/VCP mutation with differential binding pattern and subcellular localization. The international journal of biochemistry & cell biology. 2013;45:773-82.
[46] Dantuma NP, Lindsten K, Glas R, Jellne M, Masucci MG. Short-lived green fluorescent proteins for quantifying ubiquitin/proteasome-dependent proteolysis in living cells. Nat Biotechnol. 2000;18:538-43.
[47] Ye Y, Meyer HH, Rapoport TA. Function of the p97-Ufd1-Npl4 complex in retrotranslocation from the ER to the cytosol: dual recognition of nonubiquitinated polypeptide segments and polyubiquitin chains. The Journal of cell biology. 2003;162:71-84.
[48] Chou TF, Deshaies RJ. Quantitative cell-based protein degradation assays to identify and classify drugs that target the ubiquitin-proteasome system. J Biol Chem. 2011;286:16546-54.
[49] Her NG, Toth JI, Ma CT, Wei Y, Motamedchaboki K, Sergienko E, et al. p97 Composition Changes Caused by Allosteric Inhibition Are Suppressed by an On-Target Mechanism that Increases the Enzyme's ATPase Activity. Cell Chem Biol. 2016;23:517-28.
[50] Pye VE, Beuron F, Keetch CA, McKeown C, Robinson CV, Meyer HH, et al. Structural insights into the p97-Ufd1-Npl4 complex. Proceedings of the National Academy of Sciences of the United States of America. 2007;104:467-72.
[51] Gui L, Zhang X, Li K, Frankowski KJ, Li S, Wong DE, et al. Evaluating p97 Inhibitor Analogues for Potency against p97-p37 and p97-Npl4-Ufd1 Complexes. Chemmedchem. 2016;11:953-7.
[52] Conicella AE, Huang R, Ripstein ZA, Nguyen A, Wang E, Lohr T, et al. An intrinsically disordered motif regulates the interaction between the p47 adaptor and the p97 AAA+ ATPase. Proceedings of the National Academy of Sciences of the United States of America. 2020;117:26226-36.

[53] Davies JM, Brunger AT, Weis WI. Improved structures of full-length p97, an AAA ATPase: implications for mechanisms of nucleotide-dependent conformational change. Structure. 2008;16:715-26.
[54] Chapman E, Maksim N, de la Cruz F, La Clair JJ. Inhibitors of the AAA+ chaperone p97. Molecules. 2015;20:3027-49.
[55] Huryn DM, Kornfilt DJP, Wipf P. p97: An Emerging Target for Cancer, Neurodegenerative Diseases, and Viral Infections. J Med Chem. 2020;63:1892-907.
[56] Zhang G LS, Cheng KW, Chou TF. AAA ATPases as Therapeutic Targets: Structure, Functions, and Small-Molecule Inhibitors. European Journal of Medicinal Chemistry. 2021;In Press.
[57] Chou TF, Brown SJ, Minond D, Nordin BE, Li K, Jones AC, et al. Reversible inhibitor of p97, DBeQ, impairs both ubiquitin-dependent and autophagic protein clearance pathways. Proceedings of the National Academy of Sciences of the United States of America. 2011;108:4834-9.
[58] Chou TF, Li K, Frankowski KJ, Schoenen FJ, Deshaies RJ. Structure-activity relationship study reveals ML240 and ML241 as potent and selective inhibitors of p97 ATPase. Chemmedchem. 2013;8:297-312.
[59] Magnaghi P, D'Alessio R, Valsasina B, Avanzi N, Rizzi S, Asa D, et al. Covalent and allosteric inhibitors of the ATPase VCP/p97 induce cancer cell death. Nat Chem Biol. 2013;9:548-56.
[60] Zhang G, Li S, Wang F, Jones AC, Goldberg AFG, Lin B, et al. A covalent p97/VCP ATPase inhibitor can overcome resistance to CB-5083 and NMS-873 in colorectal cancer cells. Eur J Med Chem. 2021;213:113148.
[61] Wang F, Li S, Gan TP, Stott GM, Flint A, Chou TF. Allosteric p97 Inhibitors Can Overcome Resistance to ATP-Competitive p97 Inhibitors for Potential Anticancer Therapy. Chemmedchem. 2020;15:685-94.
[62] Fang CJ, Gui L, Zhang X, Moen DR, Li K, Frankowski KJ, et al. Evaluating p97 inhibitor analogues for their domain selectivity and potency against the p97-p47 complex. Chemmedchem. 2015;10:52-6.
[63] Bastola P, Wang F, Schaich MA, Gan T, Freudenthal BD, Chou TF, et al. Specific mutations in the D1-D2 linker region of VCP/p97 enhance ATPase activity and confer resistance to VCP inhibitors. Cell death discovery. 2017;3:17065.
[64] Dreveny I, Pye VE, Beuron F, Briggs LC, Isaacson RL, Matthews SJ, et al. p97 and close encounters of every kind: a brief review. Biochem Soc Trans. 2004;32:715-20.
[65] Stach L, Freemont PS. The AAA+ ATPase p97, a cellular multitool. The Biochemical journal. 2017;474:2953-76.
[66] Hanzelmann P, Schindelin H. The Interplay of Cofactor Interactions and Post-translational Modifications in the Regulation of the AAA+ ATPase p97. Frontiers in molecular biosciences. 2017;4:21.
[67] Fernandez-Saiz V, Buchberger A. Imbalances in p97 co-factor interactions in human proteinopathy. EMBO Rep. 2010;11:479-85.
[68] Ritz D, Vuk M, Kirchner P, Bug M, Schutz S, Hayer A, et al. Endolysosomal sorting of ubiquitylated caveolin-1 is regulated by VCP and UBXD1 and impaired by VCP disease mutations. Nat Cell Biol. 2011;13:1116-U148.
[69] Weith M, Seiler J, van den Boom J, Kracht M, Hulsmann J, Primorac I, et al. Ubiquitin-Independent Disassembly by a p97 AAA-ATPase Complex Drives PP1 Holoenzyme Formation. Mol Cell. 2018;72:766-77 e6.
[70] Bruderer RM, Brasseur C, Meyer HH. The AAA ATPase p97/VCP interacts with its alternative co-factors, Ufd1-Npl4 and p47, through a common bipartite binding mechanism. J Biol Chem. 2004;279:49609-16.
[71] Dreveny I, Kondo H, Uchiyama K, Shaw A, Zhang X, Freemont PS. Structural basis of the interaction between the AAA ATPase p97/VCP and its adaptor protein p47. EMBO J. 2004;23:1030-9.
[72] Yuan X, Shaw A, Zhang X, Kondo H, Lally J, Freemont PS, et al. Solution structure and interaction surface of the C-terminal domain from p47: A major p97-cofactor involved in SNARE disassembly1. J Mol Biol. 2001;311:255-63.
[73] Yuan X, Simpson P, McKeown C, Kondo H, Uchiyama K, Wallis R, et al. Structure, dynamics and interactions of p47, a major adaptor of the AAA ATPase, p97. EMBO J. 2004;23:1463-73.
[74] Cooney I, Han H, Stewart MG, Carson RH, Hansen DT, Iwasa JH, et al. Structure of the Cdc48 segregase in the act of unfolding an authentic substrate. Science. 2019;365:502-5.
[75] Twomey EC, Ji ZJ, Wales TE, Bodnar NO, Ficarro SB, Marto JA, et al. Substrate processing by the Cdc48 ATPase complex is initiated by ubiquitin unfolding. Science. 2019;365:462.
[76] Pan M, Yu YY, Ai HS, Zheng QY, Xie Y, Liu L, et al. Mechanistic insight into substrate processing and allosteric inhibition of human p97. Nature structural & molecular biology. 2021;28:614.
[77] Banerjee S, Bartesaghi A, Merk A, Rao P, Bulfer SL, Yan Y, et al. 2.3 A resolution cryo-EM structure of human p97 and mechanism of allosteric inhibition. Science. 2016;351:871-5.
[78] Xue L, Blythe EE, Freiberger EC, Mamrosh JL, Hebert AS, Reitsma JM, et al. Valosin-containing protein (VCP)-Adaptor Interactions are Exceptionally Dynamic and Subject to Differential Modulation by a VCP Inhibitor. Mol Cell Proteomics. 2016;15:2970-86.

[79] Uchiyama K, Jokitalo E, Kano F, Murata M, Zhang X, Canas B, et al. VCIP135, a novel essential factor for p97/p47-mediated membrane fusion, is required for Golgi and ER assembly in vivo. The Journal of cell biology. 2002;159:855-66.
[80] Meyer HH, Kondo H, Warren G. The p47 co-factor regulates the ATPase activity of the membrane fusion protein, p97. FEBS Lett. 1998;437:255-7.
[81] Cheng A, Eng ET, Alink L, Rice WJ, Jordan KD, Kim LY, et al. High resolution single particle cryo-electron microscopy using beam-image shift. J Struct Biol. 2018;204:270-5.
[82] Mastronarde DN. Automated electron microscope tomography using robust prediction of specimen movements. J Struct Biol. 2005;152:36-51.
[83] Punjani A, Rubinstein JL, Fleet DJ, Brubaker MA. cryoSPARC: algorithms for rapid unsupervised cryo-EM structure determination. Nat Methods. 2017;14:290-6.
[84] Bepler T, Morin A, Rapp M, Brasch J, Shapiro L, Noble AJ, et al. Positive-unlabeled convolutional neural networks for particle picking in cryo-electron micrographs. Nat Methods. 2019;16:1153-60.
[85] Punjani A, Zhang H, Fleet DJ. Non-uniform refinement: adaptive regularization improves single-particle cryo-EM reconstruction. Nat Methods. 2020;17:1214-21.
[86] Scheres SH, Chen S. Prevention of overfitting in cryo-EM structure determination. Nat Methods. 2012;9:853-4.
[87] Pettersen EF, Goddard TD, Huang CC, Couch GS, Greenblatt DM, Meng EC, et al. UCSF Chimera--a visualization system for exploratory research and analysis. J Comput Chem. 2004;25:1605-12.
[88] Emsley P, Lohkamp B, Scott WG, Cowtan K. Features and development of Coot. Acta Crystallogr D Biol Crystallogr. 2010;66:486-501.
[89] Adams PD, Afonine PV, Bunkoczi G, Chen VB, Davis IW, Echols N, et al. PHENIX: a comprehensive Python-based system for macromolecular structure solution. Acta Crystallogr D Biol Crystallogr. 2010;66:213-21.
[90] Goddard TD, Huang CC, Meng EC, Pettersen EF, Couch GS, Morris JH, et al. UCSF ChimeraX: Meeting modern challenges in visualization and analysis. Protein Sci. 2018;27:14-25.

FIGURE LEGENDS

Figure 1. p97 domain organization. (A) p97 AAA+ ATPase domains. p97 consists of an N terminal region (green; residues 1-184) containing cofactor binding sites and the disease-related, conserved arginine residue (R155), followed by the D1 (orange; residues 211-459) and D2 (orange red; residues 482-762) ATPase domains. These two domains are joined by a linker (blue; residues 460-481), containing a highly conserved leucine residue (L464). (B) Structures of the p97 monomer with the N-domain in conformations. At the left is the up-conformation (PDB code: 5FTN), and at the right is the down-conformation (PDB code: 5FTM) [77]. (C) Superposition of the crystal structure of the $p97^{ND1}$-$p47^{UBX}$ (PDB code: 1S3S) [71] with the structure of the full-length p97 in the down conformation (grey; PDB code: 5FTM). The structure of the p47-UBX is shown in pink. The distances of p47-UBX from the D1 domain, the D1-D2 linker, and the D2 domain are 34.7 Å, 47.8 Å, and 52.2 Å, respectively.

Figure 2. ATPase activity of full-length (FL) D1-D2 linker mutants and concentration-dependent effects of cofactors. (A) ATPase activity of FL p97 proteins normalized to WT activity and measured with 200 μM ATP (n=8). (B-D) ATPase activity of WT-p97 (blue) and D1-linker mutants L464E (red), L464A (green), and L464P (purple) at increasing concentrations (0-800 nM) of cofactors (B) p47 (C), p37, and (D) Npl4-Ufd1 (NU). Experiments were performed using p97 proteins at 4.17 nM hexamer and 200 μM ATP, and the activity of each p97 protein was normalized to its basal activity in the absence of cofactors (n=6). All error bars indicate ± SD.

Figure 3. Steady-state kinetic analysis of full-length D1-D2 linker mutants and cofactor-enzyme complexes. (A) Michaelis-Menten curves of ATP hydrolysis by L464P-p97 with and without cofactors (n=10). (B-D) Steady-state kinetic analyses of WT, L464A, L464E, and L464P-p97 catalyzed ATP hydrolysis performed alone (solid bar) and in the presence of 400 nM p47, p37, or Npl4-Ufd1 (NU) (n=8). Dependence of apparent k_{cat} (B), apparent K_m (C), and apparent k_{cat}/K_m (D) values on cofactors p47 (horizontal stripes), p37 (vertical stripes), and NU (checkered) are shown for WT-p97 (blue), L464A (green), L464E (red), and L464P (purple). Experiments were performed using p97 proteins at 4.17 nM hexamer and 30-750 μM ATP. All error bars indicate ± SD.

Figure 4. ATPase activity of WT-ND1L and ND1L-linker mutants and concentration-dependent effects of cofactors. (A) ATPase activity of ND1L proteins normalized to WT-ND1L (n=8). (B-D) ATPase activity of WT-ND1L (blue open triangles) and ND1L-linker mutants L464E-ND1L (red open squares) and L464P-ND1L (purple open circles) at increasing concentrations (0-800 nM) of cofactors p47 (B) (n=6), p37 (C) (*n*=12), and Npl4-Ufd1 (NU; D) (WT and L464E *n*=9; L464P *n*=4). Experiments were performed using ND1L proteins at 4.17 nM hexamer for WT and L464E, 20.85 nM hexamer for L464P-ND1L, and 200 μM ATP. All error bars indicate ± SD.

Figure 5. Steady-state kinetic analysis of WT-ND1L, ND1L-linker mutants, and cofactor-enzyme complexes. (A) Michaelis-Menten curves of ATP hydrolysis by L464P-ND1L in buffer (circles), p47 (diamonds), and p37 (triangles). (B-D) Steady-state kinetic analyses of WT, L464E, and L464P-ND1L ATP hydrolysis performed alone (solid bar) and in the presence of 400 nM p47, p37, or NU. Dependence of apparent k_{cat} (B), apparent K_m (C), and apparent k_{cat}/K_m (D) values on cofactors p47 (horizontal stripes), p37 (vertical stripes), and NU (checkered) are shown for WT-ND1L (blue), L464E-ND1L (red), and L464P-ND1L (purple).

Experiments were performed using ND1L proteins at 4.17 nM hexamer and 10-121 μM ATP. All error bars indicate ± SD and n=9.

Figure 6. Cryo-EM structural analysis of the p97^{L464P} mutant. (A) Cryo-EM density map and model of human p97^{L464P}. NTD, D1 and D2 domains are dark green, orange and orange red, respectively. Linkers and C-terminal tail are colored in grey. Outer white surface and colored surface densities are present in signal levels of 2.7$\boldsymbol{\sigma}$ and 7.6$\boldsymbol{\sigma}$, respectively. Scale bar indicates 25 Å. (B) Superposition of structures of the p97^{L464P} mutant and ADP-bound p97^{WT} (PDB code: 5FTK). The RMSD of the superimposed structures is 1.162 Å. p97^{L464P} and p97^{WT} are in blue and golden yellow, respectively. (C) Enlarged view of the mutated residues from leucine 464 (golden yellow) to proline (blue). (D) Enlarged view of the superimposed D1-D2 linkers and surrounding areas. D1-D2 linker, helix-turn-helix (HTH) motif (K543-A569) and flexible central D2 loop (586-598) are colored. Bound nucleotides are shown in sticks.

Figure 7. Effect of D1-D2 linker mutations on potency of p97 inhibitors. (A) Structures of p97 inhibitors. IC_{50} values for p97 inhibitors (B) NMS-873, (C) DBeQ, (D) ML240, (E) ML241, and (F) CB-5083 for full-length WT-p97 and L464 mutants at 200 μM ATP. All error bars indicate ± SD, and n=3.

Figure 8. Model for the role of the D1-D2 linker region in regulating p97 ATPase activity. (A) Mutation of L464 to Pro reduces basal ATPase activity of full-length p97 by 50% and binding with excess p47 cofactor inhibits p97^{WT} activity to be 80% of WT but active p97^{L464P} to be 200% of WT. (B) L464P mutation in the ND1L protein produces a severe defect, equal to that of complete truncation of the D1-D2 linker region (1.6% of p97^{WT}) and binding to excess p47 cofactor does not affect ND1L activity but enhances binding to ATP, whereas binding to L464P-ND1L affects the conformation of the D1-D2 linker of L464P and enhance activity to 19% of p97^{WT}.

Figure 1.

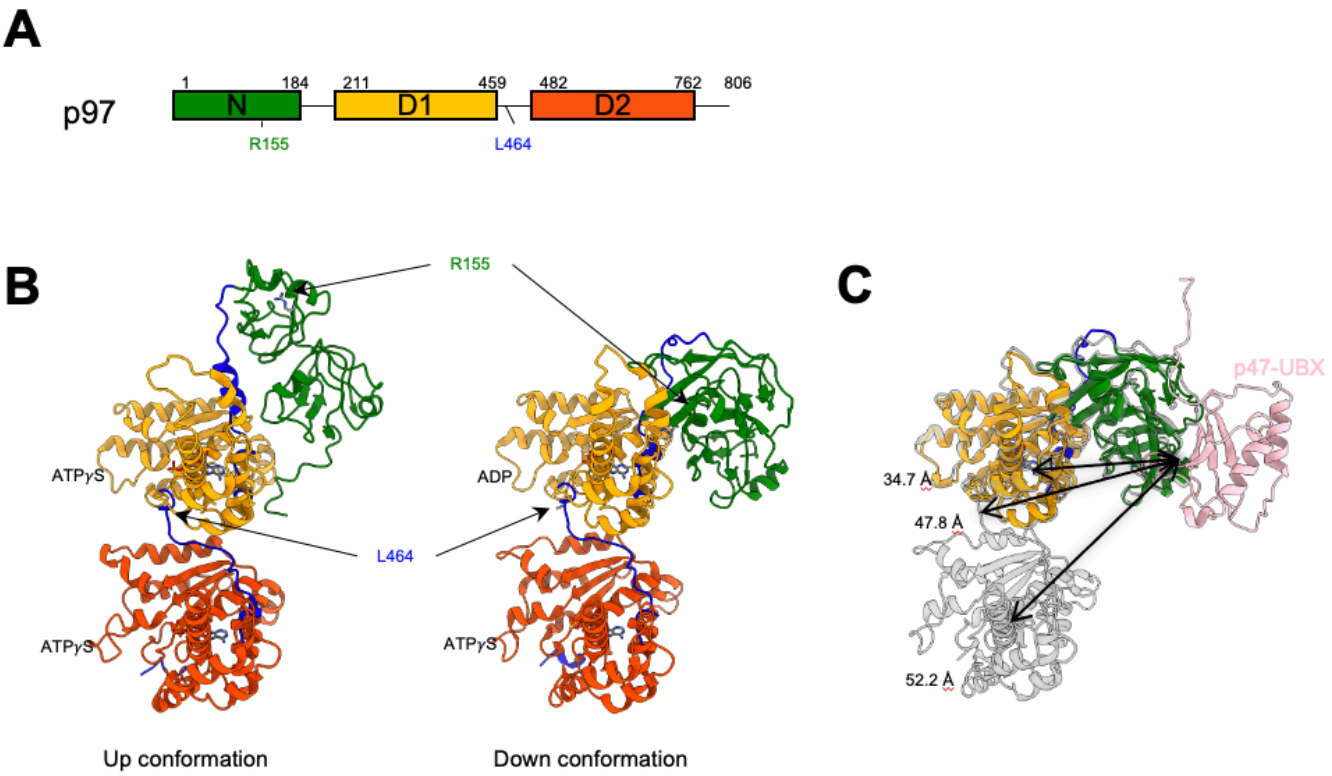

Figure 2.

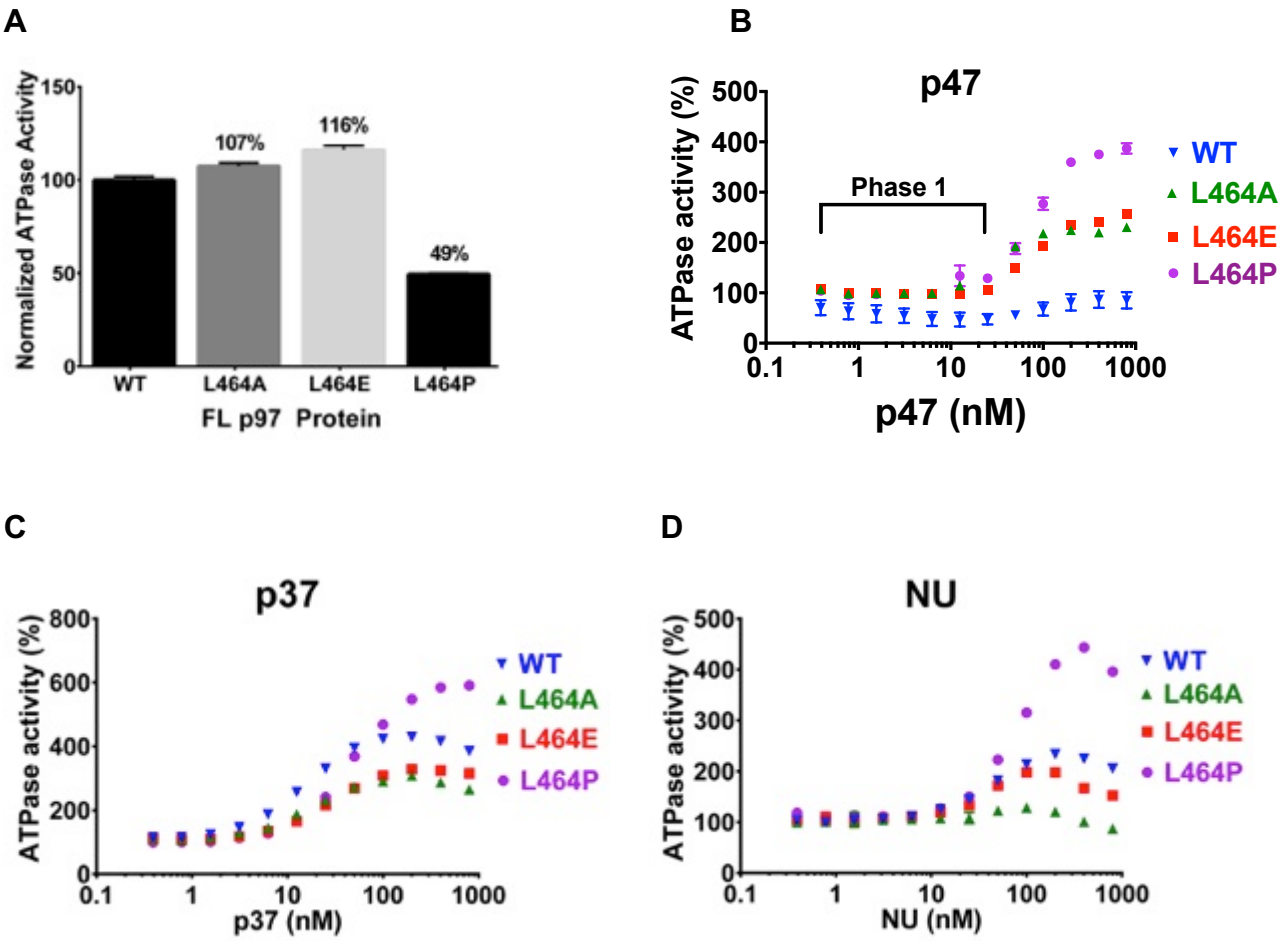

Figure 3.

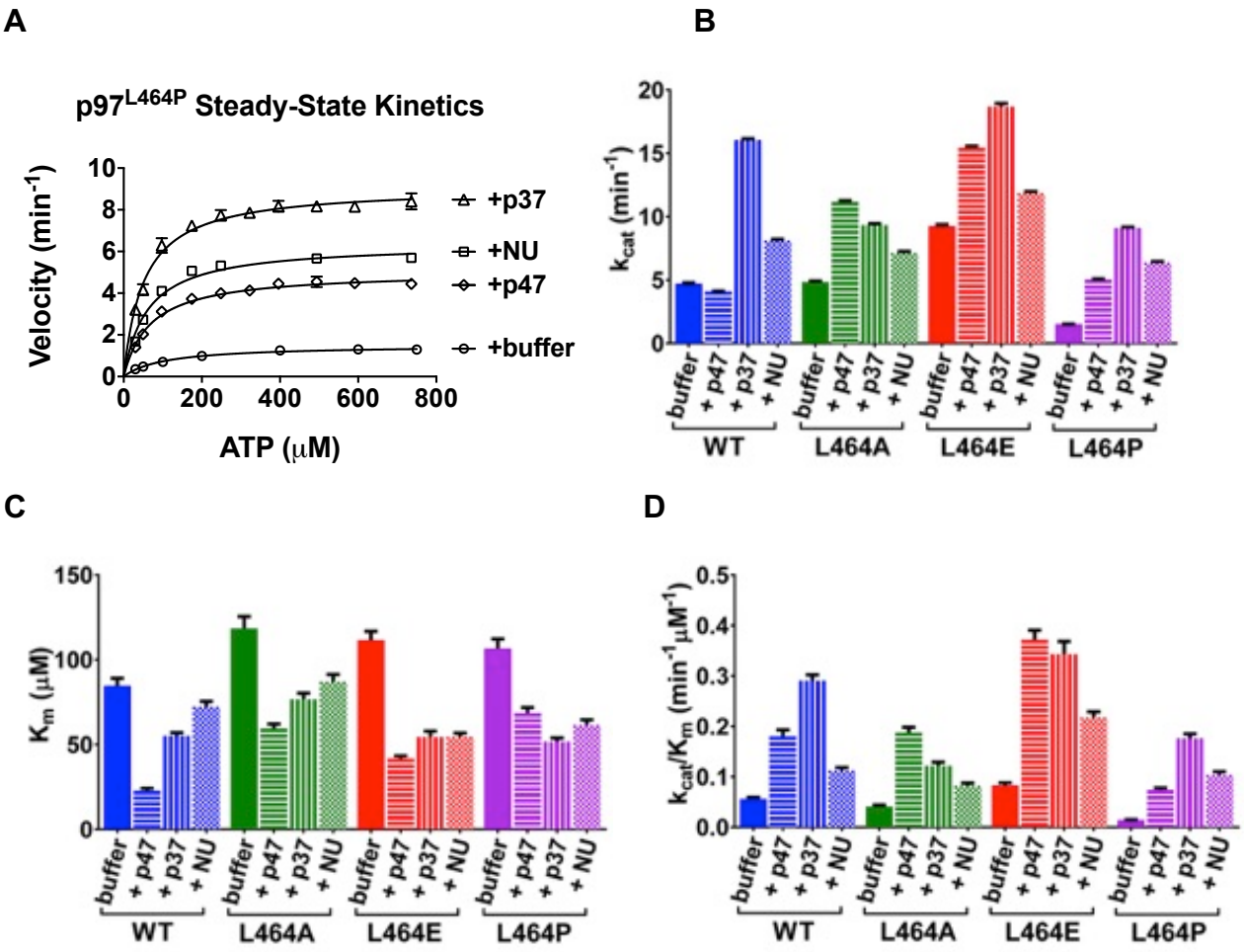

Figure 4.

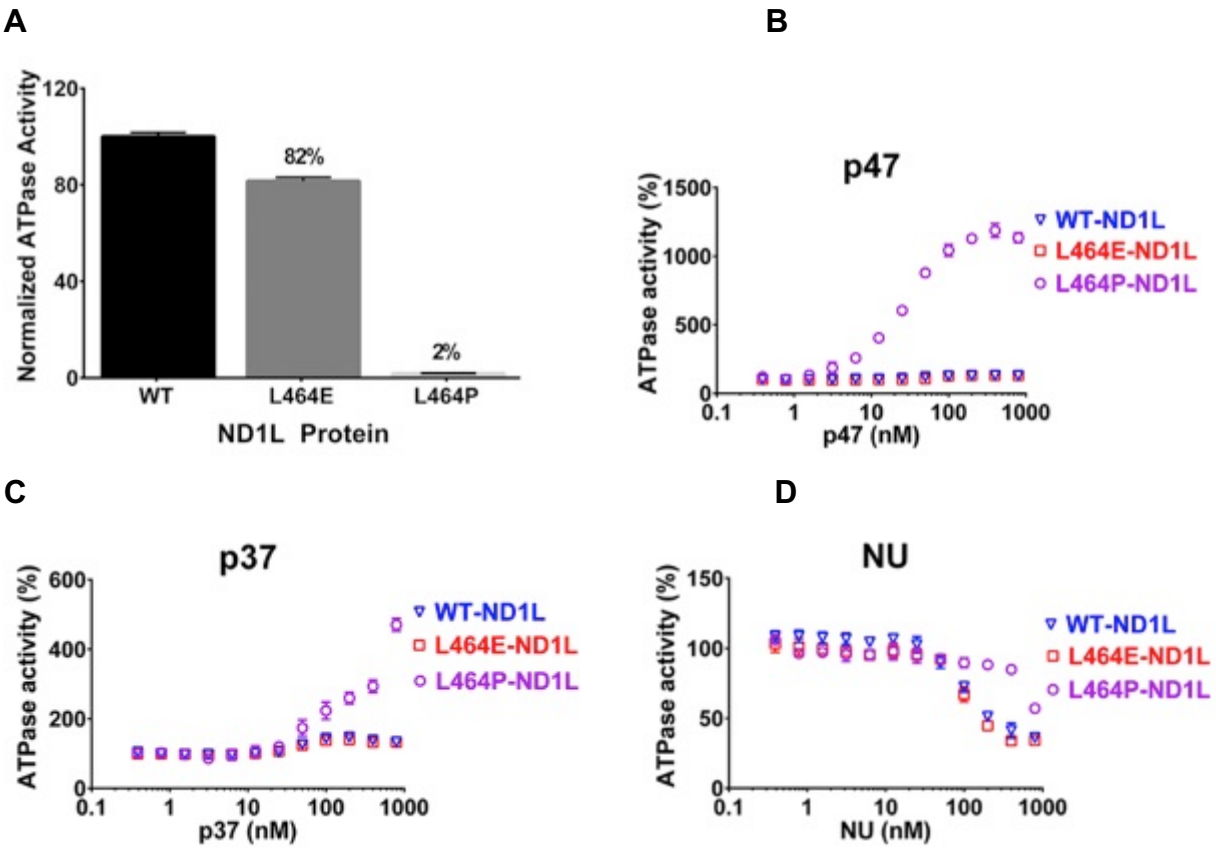

Figure 5.

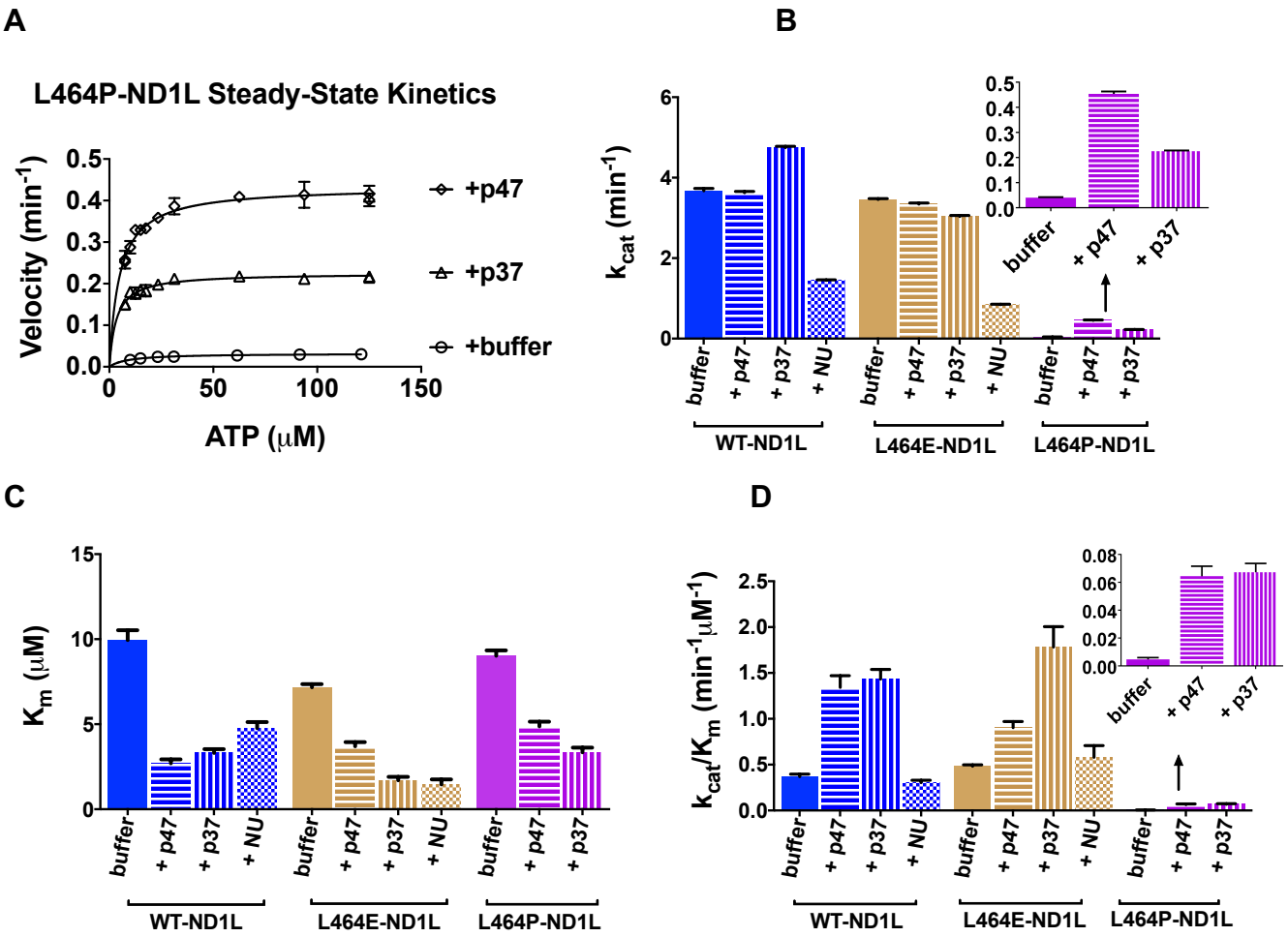

Figure 6.

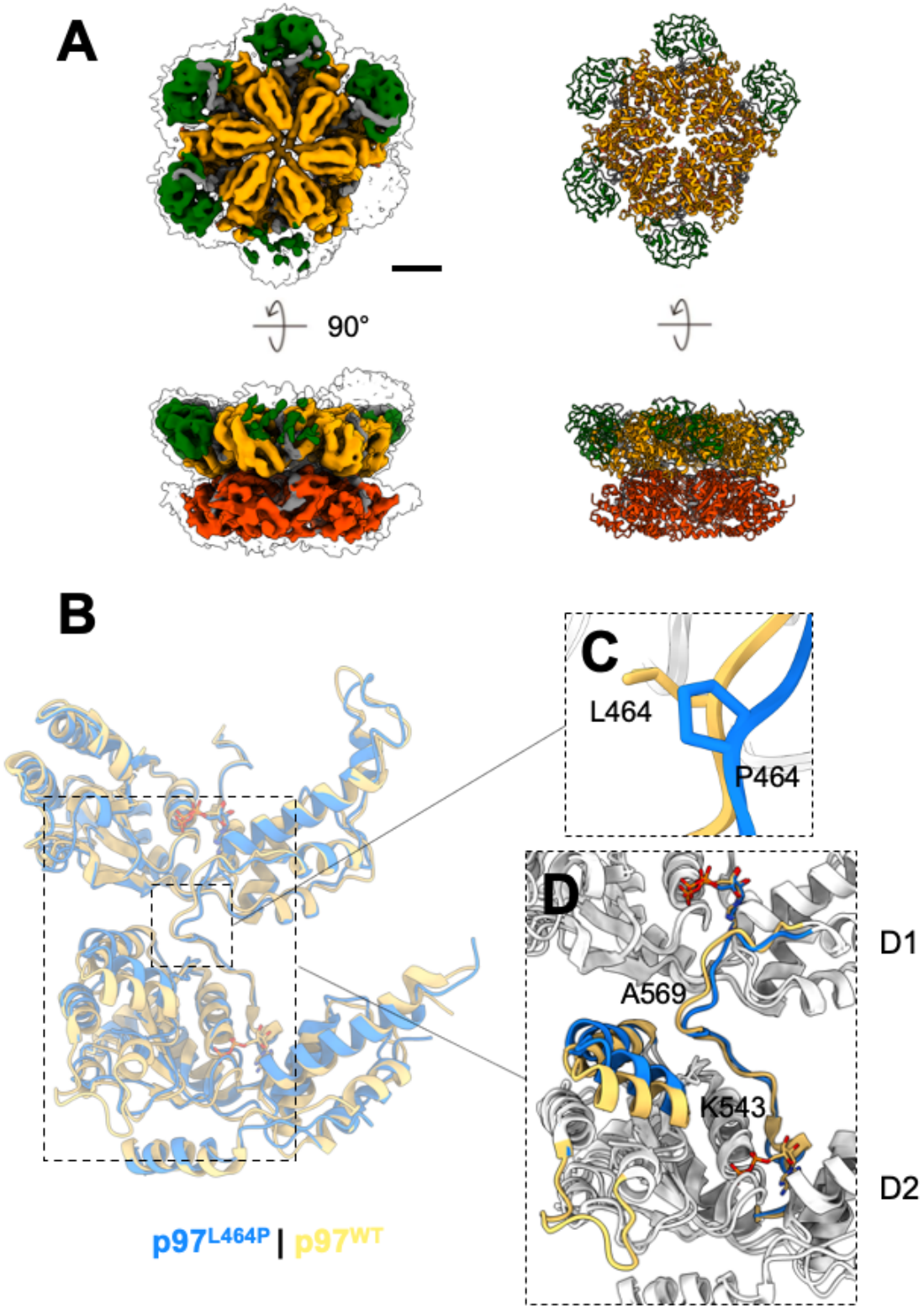

Figure 7.

A

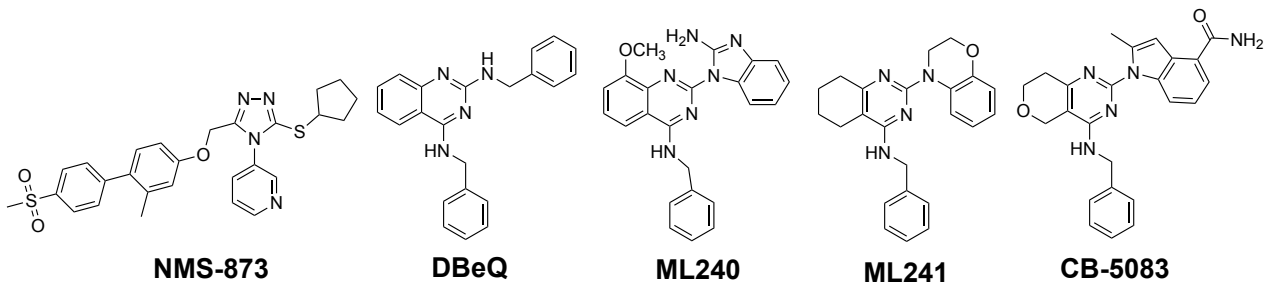

B

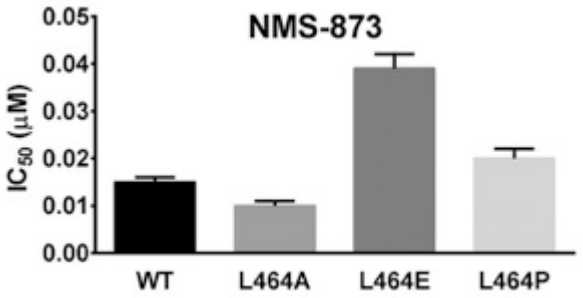

C

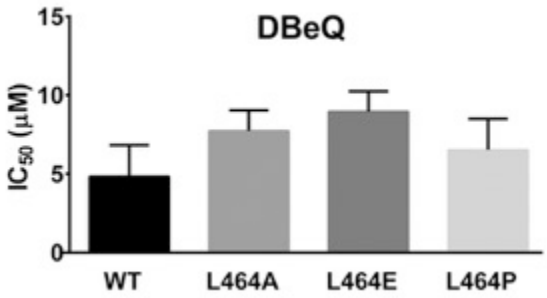

D

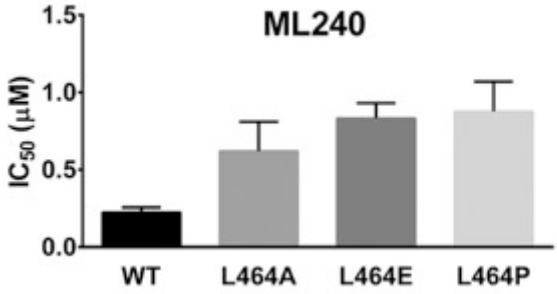

E

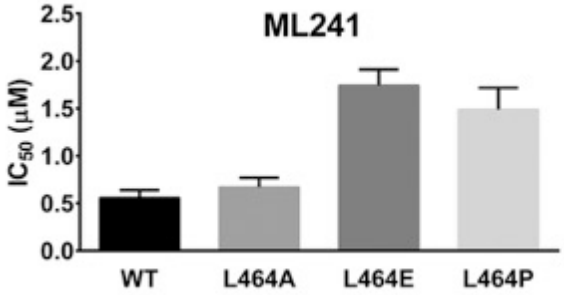

F

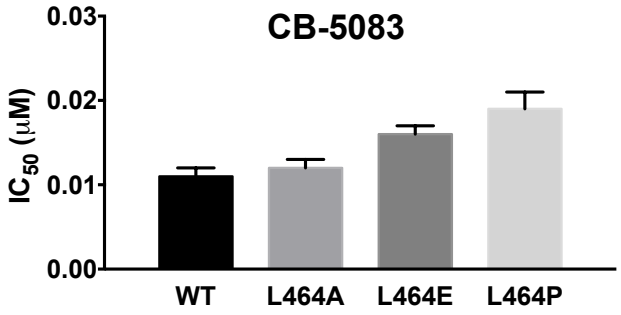

Figure 8